Journal of Solid State Chemistry 181 (2008) 1950–1960

Contents lists available at ScienceDirect

Journal of Solid State Chemistry

journal homepage: www.elsevier.com/locate/jssc

Synthesis of silicated hydroxyapatite $Ca_{10}(PO_4)_{6-x}(SiO_4)_x(OH)_{2-x}$

Mickaël Palard, Eric Champion *, Sylvie Foucaud

SPCTS, Université de Limoges, CNRS, Faculté des Sciences et Techniques, 123 Avenue Albert Thomas, 87060 Limoges Cedex, France

ARTICLE INFO

Article history:
Received 16 January 2008
Received in revised form
28 March 2008
Accepted 16 April 2008
Available online 4 May 2008

Keywords:
Powder synthesis
Silicated hydroxyapatite
Mechanisms of formation

ABSTRACT

The preparation of silicated hydroxyapatite $Ca_{10}(PO_4)_{6-x}(SiO_4)_x(OH)_{2-x}$ (SiHA) with $0 \leqslant x \leqslant 2$ was investigated using a wet precipitation method followed by a heat treatment. X-ray diffraction and Rietveld refinement, Fourier transformed IR (FTIR) spectroscopy, elemental analyses, transmission electron microscopy and thermal analyses were used to characterize the samples. The raw materials were composed of a partially silicated and carbonated apatite and a secondary minor phase containing the excess silicon. Single phase silicated hydroxyapatites, with $0 \leqslant x \leqslant 1$, could be synthesized after a thermal treatment of the raw powders above 700 °C. The presence of carbonate groups in the raw apatite played an important role in the incorporation of silicates during heating. From the different results, the mechanisms of formation of SiHA are discussed.

1. Introduction

Hydroxyapatite ($Ca_{10}(PO_4)_6(OH)_2$, HA), which chemical formula is close to that of bone mineral is commonly used as a bioceramic due to its biological properties of biocompatibility [1]. But, even if the biocompatibility of HA is excellent, its bioactivity can be improved. One way to increase it would be to use the ability of the apatite to accept many substituting ions in its unit cell [2]. Thus, the sintering of ceramics made of substituted hydroxyapatite incorporating anions of interest, such as carbonate (CO_3^{2-}) or silicate (SiO_4^{4-}), was investigated [3–7]. Several authors reported the improved bioactivity and dissolution rate of HA in the presence of silicon [8–15].

Different synthesis routes were proposed to prepare silicated hydroxyapatites, including a sol–gel procedure [16], solid-state reactions [17], hydrothermal synthesis [18,19] and controlled crystallization (also called precipitation) methods [20–23].

Gibson et al. [20] stated that the negative charge of the silicate anions substituting phosphate ones was balanced by the creation of hydroxide vacancies, leading to the following chemical formula of SiHA:

$$Ca_{10}(PO_4)_{6-x}(SiO_4)_x(OH)_{2-x} \quad \text{with } 0 \leqslant x \leqslant 2 \qquad (1)$$

The synthesis of pure SiHA powders has always been a difficulty. Ruys [16] did not succeed in preparing pure silicated hydroxyapatite via a sol–gel process without secondary phase. Beta tricalcium phosphate (β-$Ca_3(PO_4)_2$, β-TCP), silicocarnotite ($Ca_{10}(PO_4)_4(SiO_4)_2$) or alpha TCP (α-$Ca_3(PO_4)_2$) were detected whatever the silicon content might be. Arcos [17] prepared well-crystallized silicate-substituted oxyapatites without incorporation of a secondary ion, but in this case, it was not hydroxy but oxyapatites. In fact, only hydrothermal techniques and precipitation methods led to monophasic materials. The presence of an amorphous phase in the as-prepared samples which could be formed with silicon was reported [21] and the presence of carbonate groups in the apatite structure before calcination is often mentioned [19–21,23]. Some attempts were made to explain the incorporation of silicate groups in the apatite structure. Arcos [21] assumed a role of carbonate groups in the raw precipitates on the incorporation of silicates. Depending on the silicate content, two different mechanisms were proposed. At low content, silicate would substitute for carbonate during the heat treatment of the powder. At high content an expulsion of Ca^{2+} cations would occur but the way they are expulsed is not mentioned.

Finally, it appears that the preparation of pure crystallized silicated hydroxyapatite with controlled composition is still a difficulty. Though, this is of prime importance in view of further understanding the real influence of silicates on the biological behaviour of HA bioceramics. More, the mechanism of incorporation of silicates in the apatite remains unclear.

The aim of the present work was to prepare pure silicated hydroxyapatites with controlled silicate amount. The aqueous precipitation method followed by a heat treatment was investigated. Several complementary characterizations were performed by means of X-ray diffraction, Rietveld refinement, FT-infrared spectroscopy, transmission electron microscopy coupled with energy dispersive analysis and selected area electron diffraction, chemical analysis, thermal analysis, mass spectroscopy,

* Corresponding author. Fax: +33 555457586.
E-mail address: eric.champion@unilim.fr (E. Champion).

0022-4596/$ - see front matter © 2008 Elsevier Inc. All rights reserved.
doi:10.1016/j.jssc.2008.04.027

determination of the bulk density of powders. From the experimental results, the mechanisms of formation of silicated hydroxyapatite are discussed.

2. Materials and methods

2.1. Materials

The raw powders were prepared by an aqueous precipitation method using $Ca(NO_3)_2 \cdot 4H_2O$ (Sigma Aldrich, France, reagent grade), $(NH_4)_2HPO_4$ (Sigma Aldrich, reagent grade) and $Si(OCOCH_3)_4$ (Sigma Aldrich, reagent grade) as reagents. The amount of reagents was calculated assuming that one silicate ion would substitute for one phosphate ion (Eq. (1)), i.e. a constant molar ratio Ca/(P+Si) = 10/6. Table 1 collects the molar number of each reagent (n_{Ca}, n_P and n_{Si}) in the initial aqueous solutions and the expected silicon molar content per unit cell of apatite (x). According to the hypothetical chemical formula (Eq. (1)), the maximum silicon content of SiHA is $x = 2$. Thus, the value of $x = 4$ would correspond to an excess of silicon. Afterwards, the powder samples will be referred as Si_xHA.

An aqueous solution (300 mL) of $(NH_4)_2HPO_4$ and $Si(OCOCH_3)_4$ was added to 500 mL of the $Ca(NO_3)_2 \cdot 4H_2O$ solution. The reaction was carried out in a vessel placed in an Argon flowing atmosphere in order to prevent any carbonation of the powder which could result from the natural dissolution in water of CO_2 gas contained in the ambient air. The pH was kept at 9 ($\pm$0.25) by the addition of an ammonium hydroxide solution (NH_4OH) using a pH stat (Hanna Instruments). The temperature was controlled and maintained at 85 °C ($\pm$5 °C). After total addition of the $(NH_4)_2HPO_4$ and $Si(OCOCH_3)_4$ solution, the reaction mixture was stirred for 15 min. The resulting raw precipitates were centrifuged and then dried at 90 °C.

Powder samples were heated in air for 2–15 h in the temperature range 400–1000 °C in a Super Kanthal furnace using alumina crucibles. The heating rate was 20 °C min^{-1}.

2.2. Characterization methods

Fourier transformed IR (FTIR) absorption spectra of powders were obtained using a Perkin Elmer Spectrum One FTIR spectrometer. They were recorded over the 400–4000 cm^{-1} region with a resolution of 2 cm^{-1}. All the spectra were normalized in respect to the υ_4 band of phosphate (602 cm^{-1}) [24]. For the raw precipitated samples, the powders were previously washed with distilled water to remove synthesis residues.

The carbonate content of powders was determined by elemental analysis (EMIA-V 320V, HORIBA). Before analysis, the powder was washed with distilled water and then heat treated at 400 °C for 2 h in order to remove the synthesis residues. This thermal treatment did not modify the chemical composition of carbonated powders [5]. The silicon content of powders was measured by Inductively Coupled Plasma Atomic Emission Spectroscopy (ICP/AES), with a Thermo-Opteck Iris model after calcination at 1000 °C for 15 h.

The crystalline phases of powders were determined using X-ray diffraction (XRD). Powder XRD data were collected using Cu$K\alpha$ radiation on a $\theta/2\theta$ diffractometer (Siemens, model D 5000) over the range 10–50° with a step size of 0.04° and a count time of 4 s. Phases identification was achieved by comparing the diffraction patterns with International Centre for Diffraction Data (ICDD) standards (PDF cards) processed on EVA software (Brukers AXS).

The lattice parameters of HA and SiHA were determined by Rietveld refinement [25] of the X-ray diffraction data collected for raw and heat-treated powders (700–1000 °C). The refinement software Fullprof_suite was used [26]. Data sets were collected over the range 10–80° with a step size of 0.04° and a count time of 4 s. The bulk density (D_x) of the powders was calculated thanks to the theoretical atomic mass (M) and the unit cell parameters of the apatite (a and c). The theoretical atomic mass (M) was determined via the silicon content measured by ICP-AES and the chemical formula (Eq. (1)). The experimental bulk density of raw (ρ_r) and heat-treated samples (ρ_c) was measured by helium pycnometry (Micromeritics AccuPyc 1330).

Secondary electron microscopy (SEM, Jeol JSM 7400 F) was used to examine the morphology of powders. The samples were also examined by transmission electron microscopy (TEM) with a JEOL 2010 microscope. Chemical analyses were performed using energy dispersion spectroscopy (EDS) and selected area electron diffraction (SAED) patterns were recorded to investigate the crystalline structure of the powders. Intereticular distances were calculated using the following equation:

$$d_{hkl} = \frac{2 \times \lambda \times L}{D} \quad (2)$$

where λ, L and D were respectively the wavelength of the electrons (2.74×10^{-12} m), the chamber length (1 m) and the distance between two points on the diffraction patterns.

The thermal behaviour was investigated from thermogravimetry coupled with differential thermal analysis (TG/DTA) in helium flowing atmosphere (100 mL min^{-1}), using a TA Instruments SDT 2960 apparatus. The heating rate was 5 °C min^{-1}. The analysis of evolved gases was performed using a quadruple mass spectrometer (MS, Pfeiffer Vacuum Thermostar) coupled together with the previous apparatus.

Table 1
Quantities of reagents, expected Si content (x), carbonate content measured in the powders heated at 400 °C for 2 h (y CO_3^{2-}) and bulk density (ρ_r) of the raw powders

Sample	n_{Ca} (mol)	n_P (mol)	n_{Si} (mol)	x (mol)	y CO_3^{2-} (mol)	ρ_r (g cm^{-3})
HA	0.32	0.192	0	0	0.02	2.80
$Si_{0.2}HA$	0.32	0.186	0.006	0.2	0.10	2.71
$Si_{0.4}HA$	0.32	0.179	0.013	0.4	0.20	2.73
$Si_{0.6}HA$	0.32	0.173	0.019	0.6	n.d.	2.72
$Si_{0.8}HA$	0.32	0.167	0.027	0.8	0.30	2.67
$Si_{1.0}HA$	0.32	0.160	0.032	1.0	0.30	2.66
$Si_{1.5}HA$	0.32	0.144	0.048	1.5	0.43	n.d.
$Si_{2.0}HA$	0.32	0.128	0.064	2.0	0.5	2.51
$Si_{4.0}HA$	0.32	0.064	0.128	4.0	0.67	2.39

n.d. not determined.

3. Results

3.1. Raw precipitated powders

The FTIR spectra of the raw precipitated powders (Fig. 1) showed the characteristic absorption bands of a carbonated hydroxyapatite [5]. The intense bands at 1090, 1030 and 961 cm^{-1} corresponded to P–O stretching vibration modes (ν_3 and ν_1). The doublet at 603–564 cm^{-1} and the band at 472 cm^{-1} corresponded to O–P–O bending modes (ν_4 and ν_2). The bands at 3570 and 630 cm^{-1} were assigned to the stretching and vibration modes, respectively, of the hydroxide groups. The two bands at 825 and 1385 cm^{-1} were assigned to residual nitrates. They were visible and intense for the sample $Si_{2.0}HA$ because it was not washed before the analysis. The broad band between 3200 and 3700 cm^{-1} corresponded to residual H_2O adsorbed at the particle surface. The band centred at 1632 cm^{-1} was assigned to H_2O. The band at 875 cm^{-1} (Fig. 1b) and the two bands at

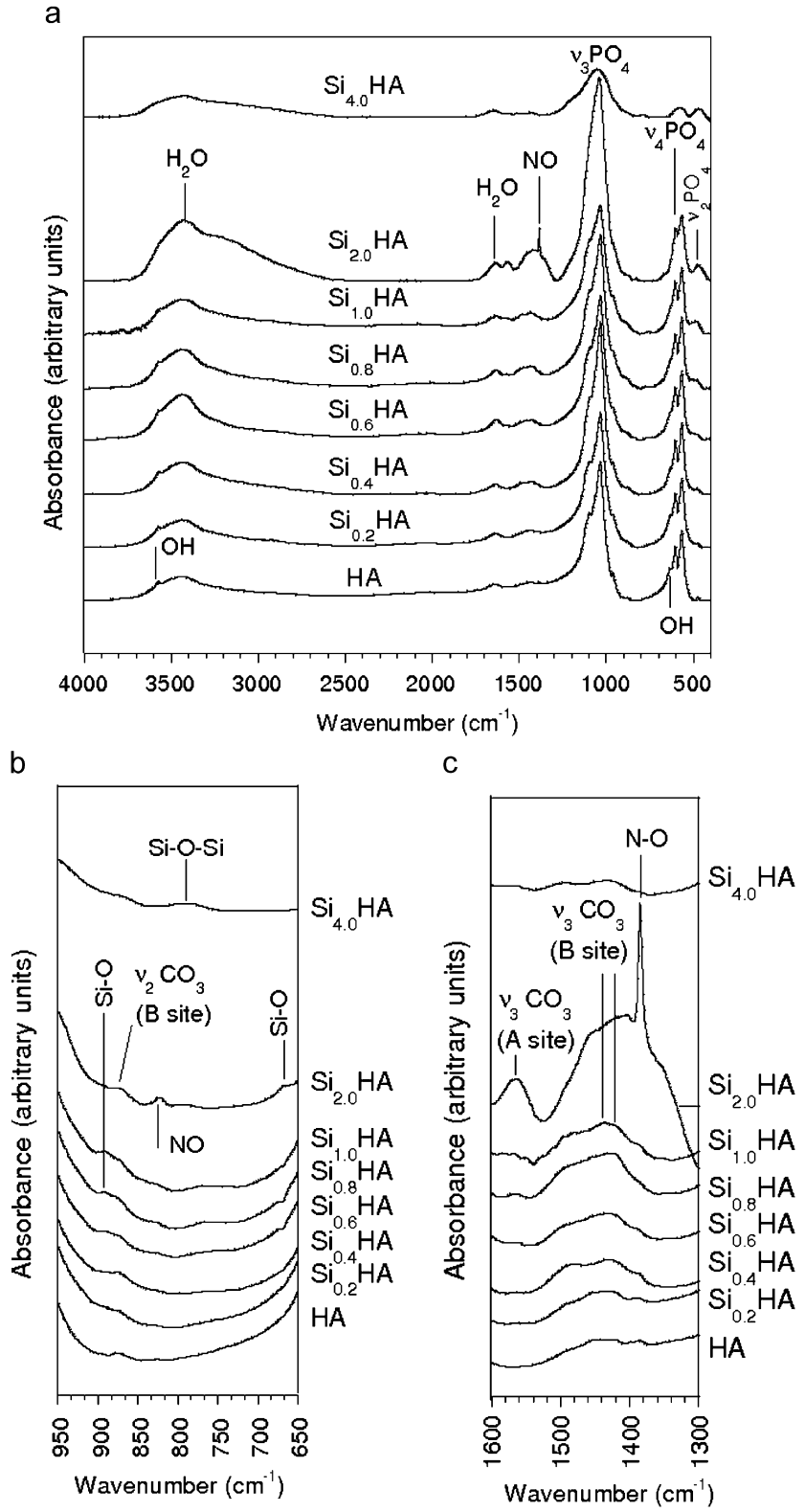

Fig. 1. FTIR spectra of the raw powders.

1420–1450 cm^{-1} (Fig. 1c) were assigned to the ν_2 and ν_3 vibrations of CO_3^{2-} groups located in the *B* site of the apatite (e.g. carbonate substituting phosphate) [5]. The composition $Si_{2.0}HA$ contained also carbonates located in the *A* site of the apatite (e.g. carbonate substituting hydroxide) with a characteristic vibration at 1552 cm^{-1} (Fig. 1c). The carbonate content measured in the powders after heat treatment at 400 °C is given in Table 1. It increased with the silicon content from HA to $Si_{2.0}HA$. This carbonation should be due to the decomposition of the silicon tetraacetate.

A band at 890 cm^{-1} (Fig. 1b) could be attributed to Si–O in SiO_4 tetrahedra in silicated hydroxyapatite for the powders with a low

silicon content ($x \leqslant 1$) [20]. For the samples $Si_{2.0}HA$ and $Si_{4.0}HA$, two other bands were observed at 670 and 790 cm^{-1} respectively. Similar bands were assigned to Si_2O_7 bridging and Si–O–Si bending in other works devoted to the synthesis of Si-stabilized TCP [27] or calcium silicate-based biomaterials [28], but they should not be attributed to silicate groups in the apatite structure.

The XRD patterns of precipitated powders are shown in Fig. 2. For an expected silicon content up to $x = 1$, the patterns of the raw powders were characteristic of crystalline apatite, matching the ICDD standard for HA (PDF 9-432). For more than $x = 1.0$, the patterns showed only two broad peaks centred at 32° and 28° (2θ). The width of the peaks was larger when the silicon content increased. The refined lattice parameters of crystallized powders ($x \leqslant 1$) are listed in Table 2. The calculated values of a, c and V_M for HA were slightly greater than those given in the PDF 9-432. When the expected silicon content increased, the parameter c did not change significantly whereas the parameter a and the unit cell volume V of the apatite increased.

The experimental bulk density (ρ_r) of the raw powders is given in Table 1. It decreased with the increase of silicon content.

The powders were examined by SEM and TEM (Fig. 3). HA and Si_xHA samples with $0 \leqslant x \leqslant 1$ were composed of small needle shaped crystals of about 10 nm large and 100 nm long (Fig. 3a). For higher values of x the morphology was very different. The crystals were round with a size of about 100–300 nm (Fig. 3b and c). At big magnification using TEM the size of crystallites could be distinguished (Fig. 3c). It was about 5 nm.

The inter-reticular distances determined from the SAED patterns (Fig. 4) and (Eq. (2)) are given in Table 3. They were compared with those given in the PDF card of HA (No 9-432). A good agreement was found for raw HA and Si_xHA powders except for the samples synthesized with $x \geqslant 2$. Indeed, the SAED patterns of crystallized $Si_{2.0}HA$ and $Si_{4.0}HA$ powders (Fig. 4c) were very close but differed slightly from the previous ones. The crystalline structure was not identified. More, a second phase was detected in the $Si_{4.0}HA$ sample. Its SAED pattern showed that it was amorphous (Fig. 4d). EDS analyses (Fig. 5) were performed on the samples. They showed the presence of calcium and phosphorus in all the samples and silicon in the crystallized domains of Si_xHA. The amorphous phase of $Si_{4.0}HA$ contained mainly silicate. As with the use of TEOS precursor [21], an excess of silicon tetraacetate in the synthesis medium could lead to its hydrolysis into $Si(OH)_4$.

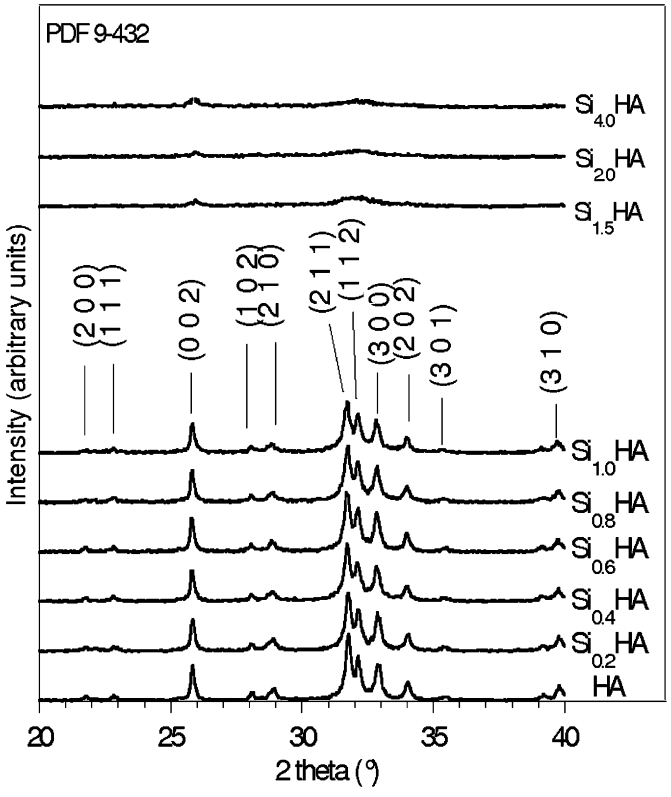

Fig. 2. XRD patterns of the raw powders.

Table 2
Lattice parameters (nm), unit cell volume (nm^3) of raw powders and powders heated at 1000 °C for 15 h

Sample	Raw precipitates			Powders heated at 1000 °C—15 h		
	a (nm)	c (nm)	V (nm^3)	a (nm)	c (nm)	V (nm^3)
HA	0.94215(7)	0.68889(4)	0.52957(7)	0.94201(6)	0.68826(9)	0.52893(9)
$Si_{0.2}HA$	0.94259(1)	0.68910(0)	0.53022(4)	0.94216(1)	0.68886(8)	0.52956(2)
$Si_{0.4}HA$	0.94306(8)	0.68922(6)	0.53085(8)	0.94217(0)	0.68970(6)	0.53021(7)
$Si_{0.6}HA$	0.94332(4)	0.68917(4)	0.53110(5)	0.94222(1)	0.69057(7)	0.53094(3)
$Si_{0.8}HA$	0.94356(9)	0.68942(6)	0.53157(7)	0.94202(0)	0.69134(4)	0.53130(7)
$Si_{1.0}HA$	0.94388(6)	0.68916(8)	0.53173(5)	0.94203(0)	0.69239(6)	0.53212(6)

3.2. Calcination

The calcinations of powders made it possible to distinguish two different behaviours depending on the silicon content.

3.2.1. Si_xHA powders with $x \leqslant 1.0$

Fig. 6 gives FTIR absorption spectra of a typical sample ($Si_{0.4}HA$) of these powders versus the temperature of calcination. The FTIR spectra were collected at room temperature. Because the powder was not washed before the analysis, the residual nitrates were detected at 825 and 1385 cm^{-1}. These residuals released during the thermal treatment disappear above 700 °C. Carbonate-free apatites were obtained above 900 °C. The decarbonation was confirmed by mass spectroscopy that showed a carbon dioxide evolution (Fig. 7) from 700 °C with a maximum near 900 °C. From the room temperature up to 700 °C, except the band at 892 cm^{-1} assigned to Si–O in SiO_4^{4-}, no other bonding containing silicate was registered. Above 700 °C, new bands appeared at 505, 753, 840 and at 945 cm^{-1}. The first three bands were assigned to Si–O in SiO_4^{4-} [20,23]. The last one was attributed to Si–OH [28].

Fig. 8 shows the XRD patterns of the composition $Si_{0.4}HA$ according to the temperature of calcination. The XRD patterns were collected at room temperature. From the room temperature up to 1000 °C, the phase kept its initial crystalline structure without formation of any secondary phase.

The influence of silicate loading was investigated using powders heat treated at 1000 °C for 15 h. Fig. 9 shows the FTIR spectra of heat-treated samples. Some of the above mentioned bands at 945, 890 and 504 cm^{-1} were present in all the compositions. Additionally, for the compositions containing up to 0.6 mol of silicon, two weak bands were observed at 840 and 750 cm^{-1}. All these bands could be attributed to silicate groups. At higher silicon loadings, two other bands appeared at about 680 and 790 cm^{-1} as in the raw $Si_{2.0}HA$ and $Si_{4.0}HA$ powders. They could be attributed to silicate in the apatite structure. Finally, the relative intensity of the band assigned to OH at 630 cm^{-1} decreased with the silicate content.

The XRD patterns of heat-treated powders (Fig. 10) showed that for a silicon content up to $x = 0.8$, the powders remained monophasic with the crystalline structure of hydroxyapatite. No secondary crystalline phase was detected. But, due to the measurements precision, traces of a second phase in amount

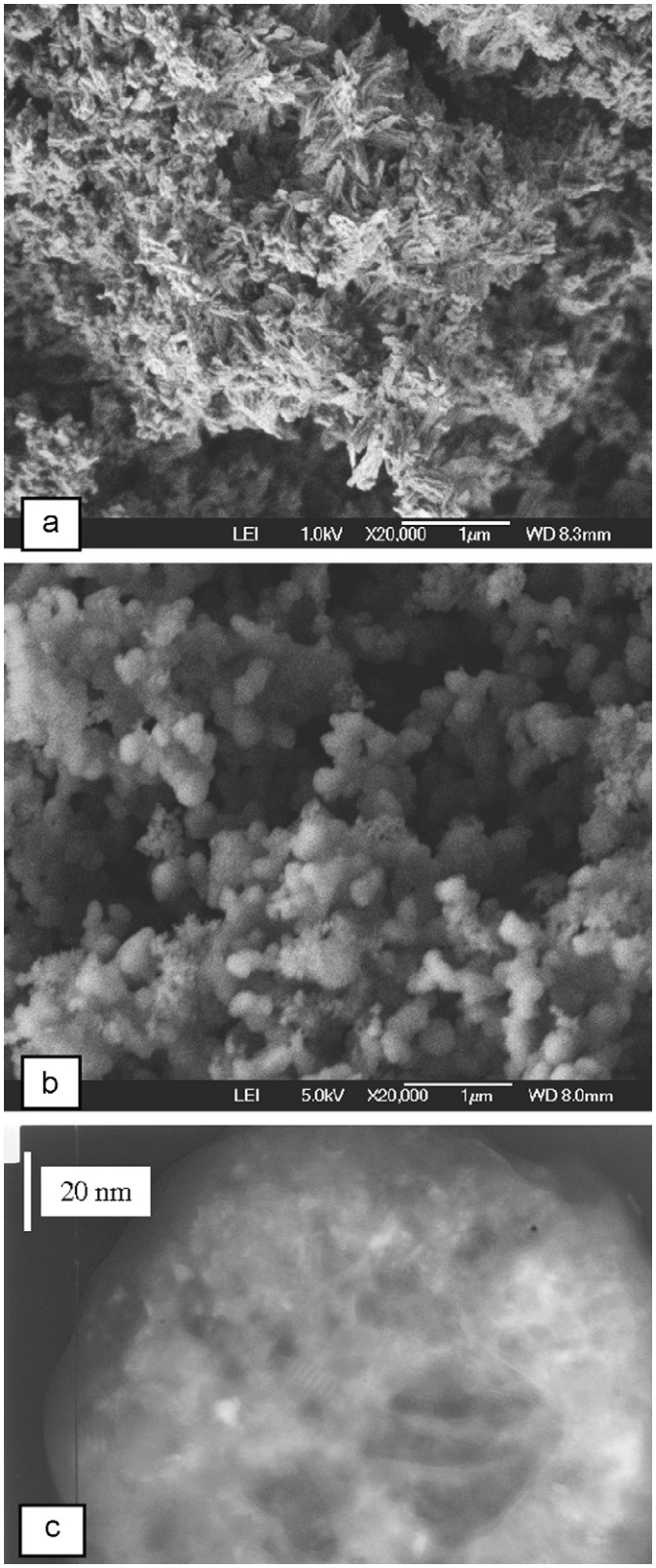

Fig. 3. SEM micrographs of $Si_{0.4}HA$ (a) and $Si_{4.0}HA$ (b). TEM micrograph of $Si_{2.0}HA$ (c).

below or around the detection limit could not be excluded. For $x = 1.0$, the powder was unambiguously biphasic, composed of hydroxyapatite (HA) and alpha tricalcium phosphate (α-TCP, PDF 9-348). However, up 1000 °C, this composition remained monophasic with the structure of hydroxyapatite, like the other Si_xHA compositions. The α-TCP phase was one of the products of the thermal decomposition of the silicated hydroxyapatite. The thermal decomposition of silicated hydroxyapatites will not be detailed here; this should be made in a forthcoming paper.

Table 2 collects the lattice parameters and the unit cell volume calculated for the apatite phase after calcinations at 1000 °C for 15 h. The parameters *a* and *c* and the unit cell volume of the powders containing up to 0.6 mol of silicon increased with the silicon content. For higher silicon loadings, the parameter *c* and the unit cell volume went on increasing, whereas the parameter *a* retook the value measured for pure HA.

The silicon content measured by ICP-AES (Table 4) was identical to the expected value. The hypothetical chemical formula, calculated thanks to the measured silicon content and (Eq. (1)) are also reported in Table 1. The calculated density (D_x) of the heat-treated powders (1000 °C—15 h) and the measured values (ρ_c) were in very good agreement (Table 4), which confirmed the absence of secondary phase in the final powders.

3.2.2. Si_xHA powders with $x > 1.0$

Fig. 11 shows the FTIR absorption spectra of the sample $Si_{2.0}HA$ after calcination at different temperatures. Carbonate-free apatites were obtained above 800 °C. From 700 °C, new bands appeared at 496 and 863 cm^{-1}. They were assigned to Si–O in the SiO_4^{4-} tetrahedron. Other bands at 732 and 990 cm^{-1} were also detected that corresponded to P–O vibrations in TCP [27,29]. More, a split of the ν_4PO_4 bands at 600–615 and 570–582 cm^{-1} was clearly observed at 1000 °C and assigned to PO_4 vibrations in HA (600 and 570 cm^{-1}) and α-TCP (615 and 582 cm^{-1}).

XRD patterns (Fig. 12) confirmed that the behaviour of Si_xHA powders with $x > 1$ was very different from that of the compositions with $x \leqslant 1$. During the thermal treatment, two phases appeared simultaneously from 700 °C. They were identified as apatite and alpha tricalcium phosphate (α-TCP).

The influence of silicate loading was investigated after heat treatment at 1000 °C for 15 h. Fig. 13 gives the FTIR spectra of the Si_xHA samples ($1.5 \leqslant x \leqslant 4$). All the powders exhibited the same Si–O vibrations as those described above for $Si_{2.0}HA$. Moreover, the band assigned to hydroxide groups at 630 cm^{-1} detected in the powders containing a low amount of silicon ($x \leqslant 1$) was no more present in these powders highly loaded in silicon. For the composition $Si_{4.0}HA$, the XRD pattern (Fig. 14) was still formed with broad peaks indicating a very low crystallinity even after the thermal treatment. The heated powder remained very similar to the raw powder. As hypothesized by other authors [21] a glassy phase could be formed from the polycondensation of the $Si(OH)_4$ secondary phase into amorphous silica. Table 4 summarizes the chemical composition of Si_xHA powders with $x > 1$.

4. Discussion

The synthesis of silicated apatites can be performed by an aqueous precipitation technique conventionally used for the preparation of other substituted hydroxyapatite powders [30,31]. Nevertheless, the production of pure crystallized silicated hydroxyapatite requires an additional thermal treatment of the raw precipitates and the silicate substitution cannot exceed 1 mol. Over this amount a secondary phase is always present in the powder. Consequently, the discussion will focus on the analysis of the formation and the properties of pure silicated hydroxyapatites, i.e. powders containing up to 1 mol of silicon.

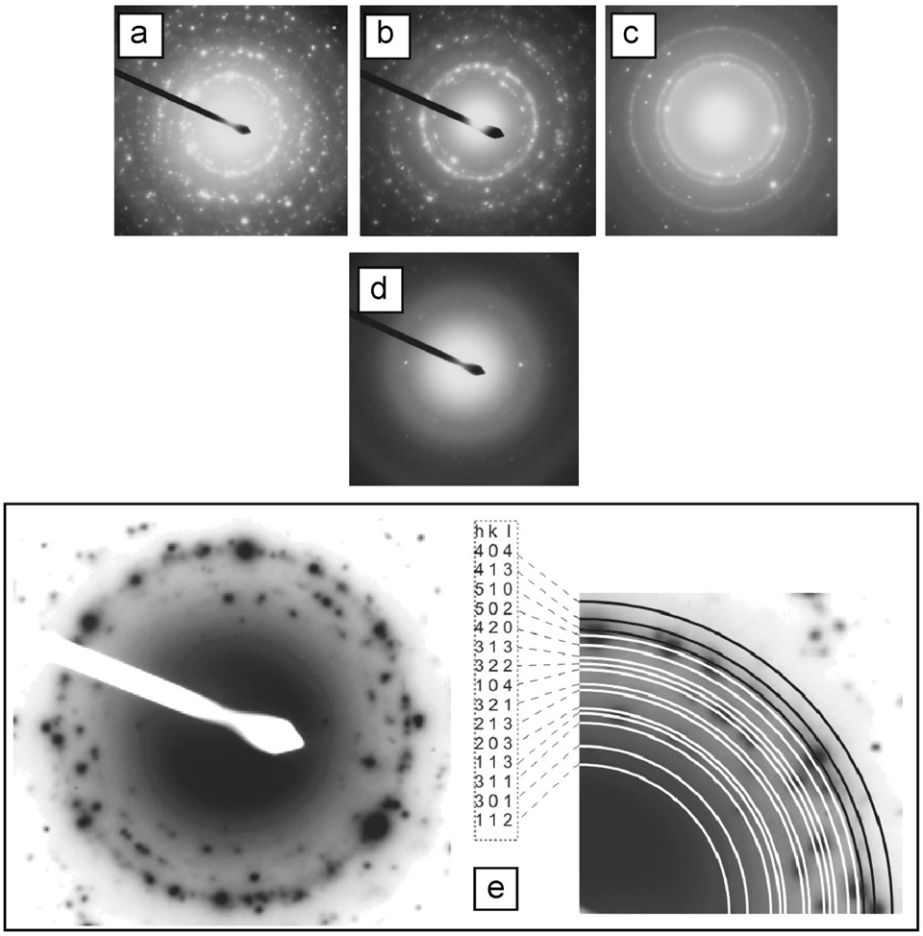

Fig. 4. SAED patterns of HA (a, e), $Si_{0.4}HA$ (b), crystallized phase in $Si_{4.0}HA$ (c) and amorphous phase in $Si_{4.0}HA$ (d).

Table 3
Inter-reticular distances of SAED patterns

Indexation *hkl*	HA		$Si_{0.4}HA$	
	d_{hkl} (Å) measured	d_{hkl} (Å) calculated	d_{hkl} (Å) measured	d_{hkl} (Å) calculated
112	2.771	2.778	2.771	2.778
301	2.514	2.528	–	–
311	2.166	2.148	–	–
113	2.067	2.065	–	–
400	–	–	2.036	2.040
203	2.016	2.000	–	–
213	1.851	1.841	1.851	1.841
321	1.802	1.806	1.786	1.806
104	1.697	1.684	1.697	1.684
322	1.656	1.644	1.656	1.644
313	1.616	1.611	1.603	1.611
420	1.543	1.542	–	–
502	1.486	1.474	1.486	1.474
510	1.460	1.465	1.465	1.465
413	1.404	1.407	1.404	1.407
422				
404	1.327	1.316	1.349	1.316
431				

4.1. Precipitation of Si_xHA raw powders ($x \leqslant 1$)

The characterizations showed that the raw precipitates had the apatite structure. All the powders were partially carbonated and silicated. As the carbonate groups were in the *B* site of the apatite structure, all the initial silicon could not be in the apatite cell after precipitation. Indeed, the quantities of reagents were calculated assuming that *x* silicate would substitute for *x* phosphate according to Eq. (1). On the hypothesis that the *B* site must be fully occupied, i.e. containing six ionic groups, and that all the initial phosphate (i.e. 6-*x* mol) is in this site, the real composition for the *B* site of the apatite is as follows:

$$(PO_4)_{6-x}(CO_3)_y(SiO_4)_w \quad (3)$$

In this case the amount of silicate incorporated in the apatite is only

$$w = x - y \quad (4)$$

where *y* represents the molar number of carbonate. Thus, a part of the initial silicon, equivalent to the *y* mole of carbonate, must be in a secondary phase in the raw precipitate.

From the composition of the *B* site (Eq. (4)), two cases can be hypothesized to write the chemical composition of the apatite phase and consequently that of the secondary phase containing the *y* mol of remaining silicon.

(i) The apatite can be defined as a solid solution of two solid solutions: a carbonated HA $Ca_{10-y}(PO_4)_{6-y}(CO_3)_y(OH)_{2-y}$ and a silicated HA $Ca_{10}(PO_4)_{6-w}(SiO_4)_w(OH)_{2-w}$. The resulting chemical formula is

$$Ca_{10-y}(PO_4)_{6-x}(CO_3)_y(SiO_4)_w(OH)_{2-x} \quad (5)$$

with $x = w+y$ (Eq. (4)). In this case the *B* site substitutions imply the creation of calcium and hydroxide vacancies to maintain the charge balance of the apatite cell according to the

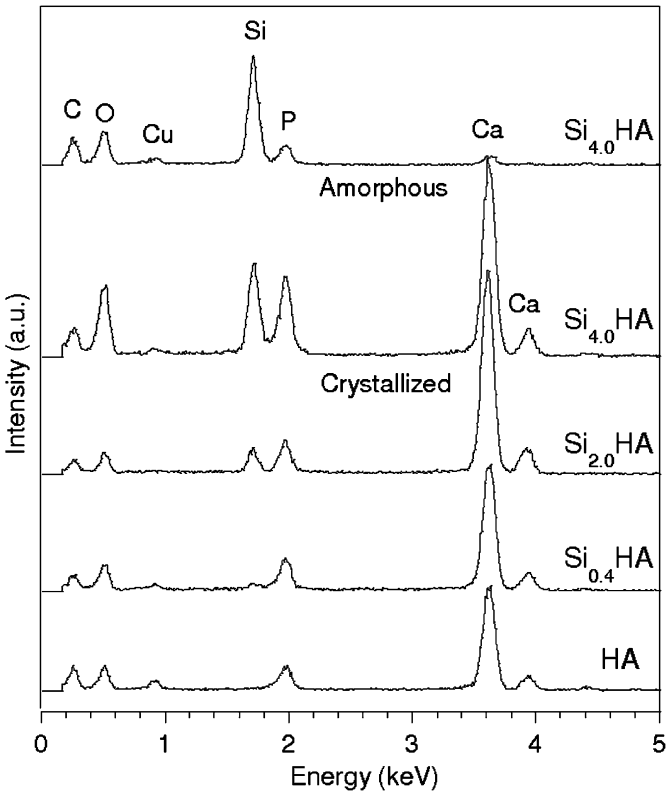

Fig. 5. EDS analyses of the raw powders.

following global mechanism:

$$y\mathrm{CO}^{\circ}_{3\mathrm{PO}_4} + (x-y)\mathrm{SiO}'_{4\mathrm{PO}_4} = x\mathrm{PO}^{\times}_{4\mathrm{PO}_4} + y\mathrm{V}''_{\mathrm{Ca}} + x\mathrm{V}^{\circ}_{\mathrm{OH}} \quad (6)$$

This hypothesis means that y mol of calcium and silicon must be in a second phase. In order to identify this phase, a complementary experiment was conducted using the same conditions as those described in Section 2.1 for the synthesis of Si_xHA powders but without phosphate solution. The precipitation was performed by adding a solution of silicon tetraacetate in a solution of calcium nitrate having the same concentration. The resulting precipitate was analysed by XRD (Fig. 15). The raw powder was poorly crystallized, but after thermal treatment of crystallization the powder was identified as wollastonite $CaSiO_3$ (PDF 43-1460). From this experiment, it was concluded that calcium and silicon, in equal quantity, that were not incorporated in the apatite during the synthesis of Si_xHA powders could have precipitated in this form of a low crystallized calcium silicate leading to the following mixture for the raw powder:

$$\mathrm{Ca}_{10-y}(\mathrm{PO}_4)_{6-x}(\mathrm{CO}_3)_y(\mathrm{SiO}_4)_w(\mathrm{OH})_{2-x} + y\mathrm{CaSiO}_3 \quad (7)$$

As the maximum value of y is equal to 0.5 mol (Table 1), the maximum relative quantity of calcium silicate in the raw powder is less than 4 wt%. The very low amount and low crystallinity of this phase may explain that is was not directly detected by the characterization means presented in the previous sections.

(ii) A second mechanism of charge balance of the apatite cell can be hypothesized. The dual substitution of carbonate and silicate can lead to a mutual charge balance according to the following mechanism:

$$\mathrm{CO}^{\circ}_{3\mathrm{PO}_4} + \mathrm{SiO}'_{4\mathrm{PO}_4} = 2\mathrm{PO}^{\times}_{4\mathrm{PO}_4} \quad (8)$$

This mechanism involved that the number of moles of silicate incorporated in apatite is identical to that of carbonate. Thus $w = y = x/2$. In this hypothesis no vacancy is created in the lattice of the apatite and the chemical formula of the raw apatitic phase could be written as follows:

$$\mathrm{Ca}_{10}(\mathrm{PO}_4)_{6-2y}(\mathrm{CO}_3)_y(\mathrm{SiO}_4)_y(\mathrm{OH})_2 \quad (9)$$

Below $x = 0.4$, the measured carbonate content y (Table 1) makes it possible to hypothesize this mechanism. But above this value of $x = 0.4$, the measured carbonate content y is less than $x/2$. Thus, more than y silicate must be incorporated to fill the B site of the apatite up to six ionic groups. The excess charge of these additional silicate groups (u) has to be balanced by the creation of hydroxide vacancies leading to the following mechanism:

$$y\mathrm{CO}^{\circ}_{3\mathrm{PO}_4} + (y+u)\mathrm{SiO}'_{4\mathrm{PO}_4} = (2y+u)\mathrm{PO}^{\times}_{4\mathrm{PO}_4} + u\mathrm{V}^{\circ}_{\mathrm{OH}} \quad (10)$$

and the resulting chemical formula of the apatite phase is

$$\mathrm{Ca}_{10}(\mathrm{PO}_4)_{6-2y}(\mathrm{CO}_3)_y(\mathrm{SiO}_4)_{y+u}(\mathrm{OH})_{2-u} \quad (11)$$

In any case, Eqs. (9) or (11), y mol of silicon (i.e. the quantity of carbonate in B site) is not incorporated into the apatite, but as there is not creation of calcium vacancy, all the calcium is in the apatite. The excess silicon must be, here again, in a secondary phase. This phase should be similar to that detected in the powder $Si_{4.0}$HA that was synthesized with $x = 4$, i.e. with a great excess of silicon. Thus, it could be amorphous $Si(OH)_4$ and the powder mixture would be

$$\mathrm{Ca}_{10}(\mathrm{PO}_4)_{6-2y}(\mathrm{CO}_3)_y(\mathrm{SiO}_4)_y(\mathrm{OH})_2\, y\ \mathrm{Si(OH)}_4 \text{ or } \mathrm{Ca}_{10}(\mathrm{PO}_4)_{6-2y}(\mathrm{CO}_3)_y(\mathrm{SiO}_4)_{y+u}(\mathrm{OH})_{2-u} + y\ \mathrm{Si(OH)}_4 \quad (12)$$

As the maximum value of y is equal to 0.5 mol (Table 1), the maximum relative quantity of silicon hydroxide in the raw powder would be less than 4 wt%. Again, the very low amount and low crystallinity of this phase may explain that is was not directly detected in the raw Si_xHA powders containing few silicon ($x \leqslant 1$) by the characterization means presented in the previous sections.

4.2. Calcination of Si_xHA powders ($x \leqslant 1$)

During the heat treatment, the decarbonation and simultaneous formation of pure crystallized silicated hydroxyapatite was shown. The formation of these silicated apatites results from a reaction between the carbonated apatite and the secondary silicon containing phase. The two compositions Eqs. (7) and (12) must be distinguished.

(i) Composition (Eq. (7))
The following reaction would occur:

$$\mathrm{Ca}_{10-y}(\mathrm{PO}_4)_{6-x}(\mathrm{CO}_3)_y(\mathrm{SiO}_4)_w(\mathrm{OH})_{2-x} + y\ \mathrm{CaSiO}_3 \rightarrow \mathrm{Ca}_{10}(\mathrm{PO}_4)_{6-x}(\mathrm{SiO}_4)_x(\mathrm{OH})_{2-x} + y\ \mathrm{CO}_2 \quad (13)$$

and the mechanism of formation of the SiHA can be written as

$$y\mathrm{CO}^{\circ}_{3\mathrm{PO}_4} + y\mathrm{V}''_{\mathrm{Ca}} + y\mathrm{CaSiO}_3 = y\mathrm{Ca}^{\times}_{\mathrm{Ca}} + y\mathrm{SiO}'_{4\mathrm{PO}_4} + y\mathrm{CO}_2 \quad (14)$$

The calcium and silicate of the secondary phase are totally incorporated in the apatite with a CO_2 gas evolution and the chemical formula of the final powder is (Eq. (1)):

$$\mathrm{Ca}_{10}(\mathrm{PO}_4)_{6-x}(\mathrm{SiO}_4)_x(\mathrm{OH})_{2-x}$$

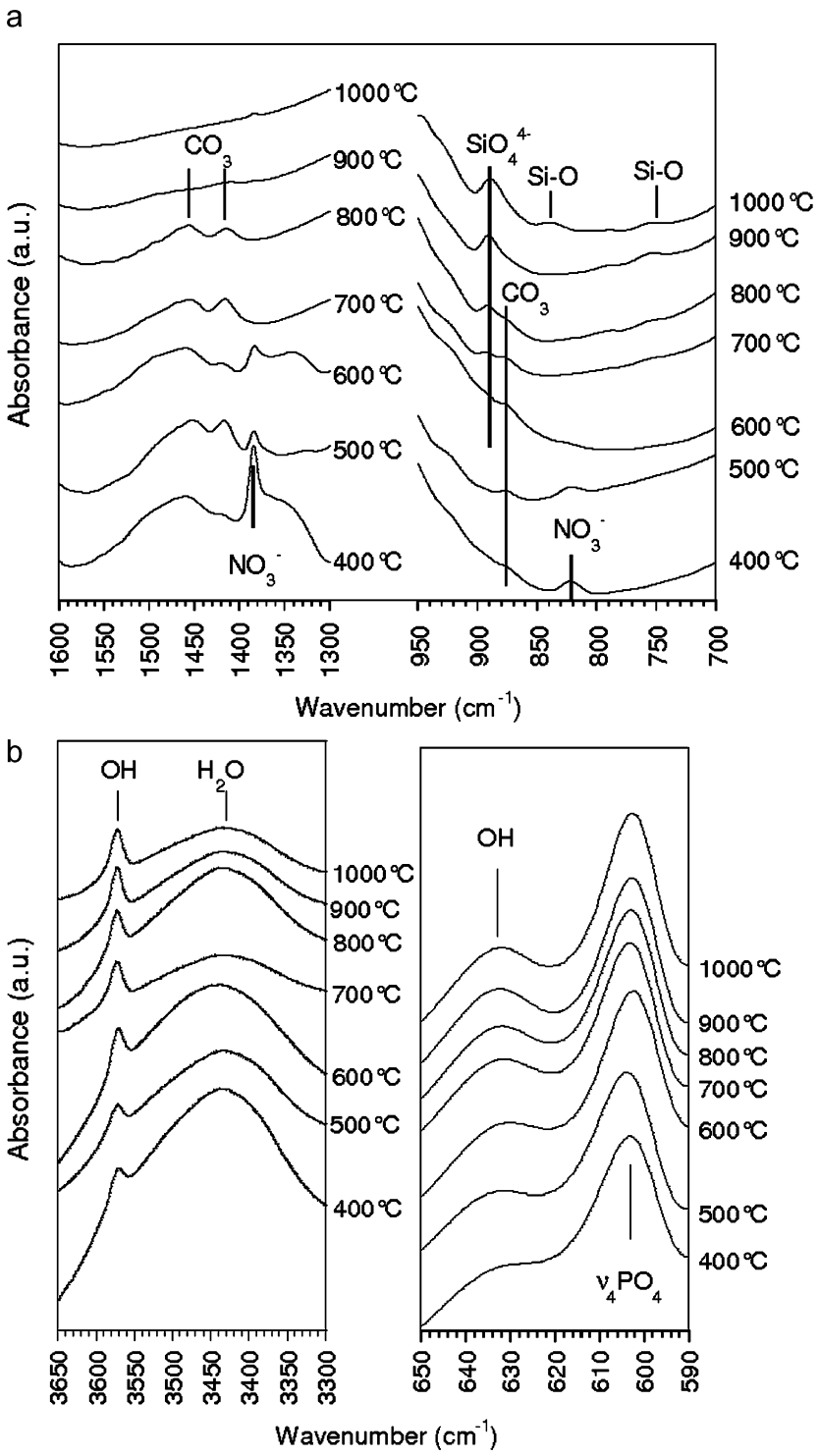

Fig. 6. FTIR spectra of $Si_{0.4}HA$ versus the temperature of calcination. (a) Vibrations of carbonate and silicate. (b) Vibrations of hydroxide.

(ii) Composition (Eq. (12))
Depending on the formulation of the initial apatite the following reactions may occur:

$$Ca_{10}(PO_4)_{6-2y}(CO_3)_y(SiO_4)_y(OH)_2 + ySi(OH)_4 \rightarrow Ca_{10}(PO_4)_{6-x}(SiO_4)_x(OH)_{2-x} + yCO_2 + 3yH_2O \quad (15)$$

$$Ca_{10}(PO_4)_{6-2y-u}(CO_3)_y(SiO_4)_{y+u}(OH)_{2-u} + ySi(OH)_4 \rightarrow Ca_{10}(PO_4)_{6-x}(SiO_4)_x(OH)_{2-x} + yCO_2 + 3yH_2O \quad (16)$$

In both cases, (15) or (16), the mechanism of formation of the SiHA can be written as

$$yCO^{\circ}_{3PO_4} + uV^{\circ}_{OH} + ySi(OH)_4 = ySiO'_{4PO_4} + 2yV^{\circ}_{OH} + yCO_2 + 3yH_2O \quad (17)$$

The incorporation of silicate in the apatite occurs with the creation of hydroxide vacancies and the evolution of CO_2 and H_2O gases. When all the silicate groups are incorporated ($x = 2y$ or

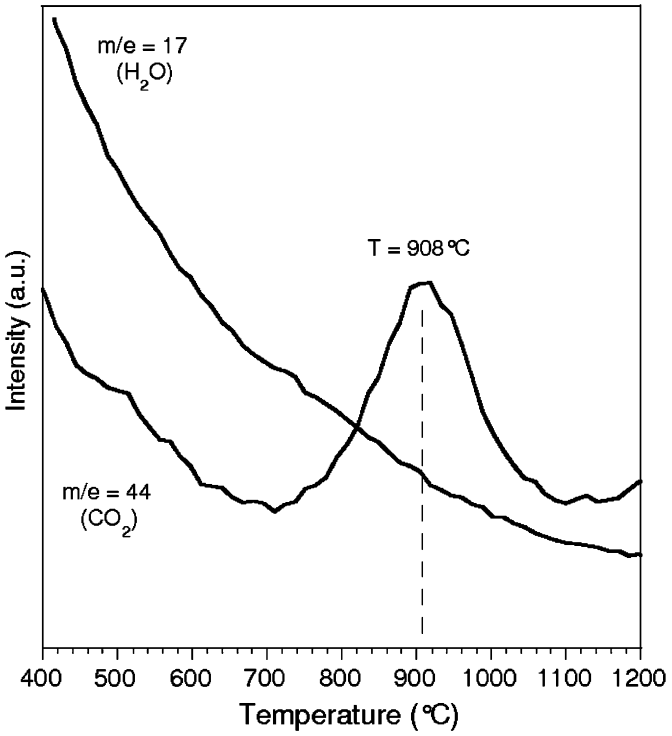

Fig. 7. Mass spectroscopy of $Si_{0.4}HA$ versus the temperature.

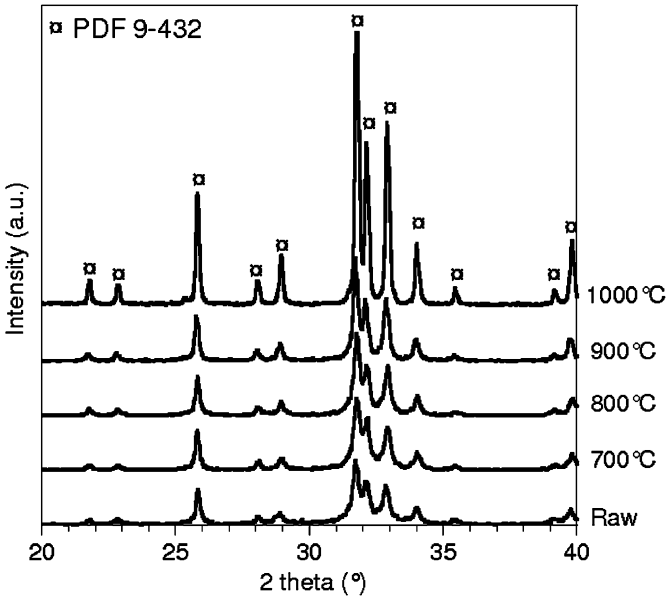

Fig. 8. XRD patterns of $Si_{0.4}HA$ versus the temperature.

$x = 2y+u$), the chemical formula of the powder is (Eq. (1))

$$Ca_{10}(PO_4)_{6-x}(SiO_4)_x(OH)_{2-x}$$

Experimentally, a carbon dioxide evolution was detected by mass spectrometry but there was no water vapour release (Fig. 7) during the calcination of the raw powders. More, there was no evidence for any creation of hydroxide vacancy since the relative intensity of the typical IR bands assigned to OH at 630 and 3570 cm^{-1} did not change during heating (Fig. 6b). Finally, the experimental results agree with the first chemical composition of the raw powder (Eq. (7)) and the mechanism of formation of pure Si_xHA during the calcinations (Eq. (14)).

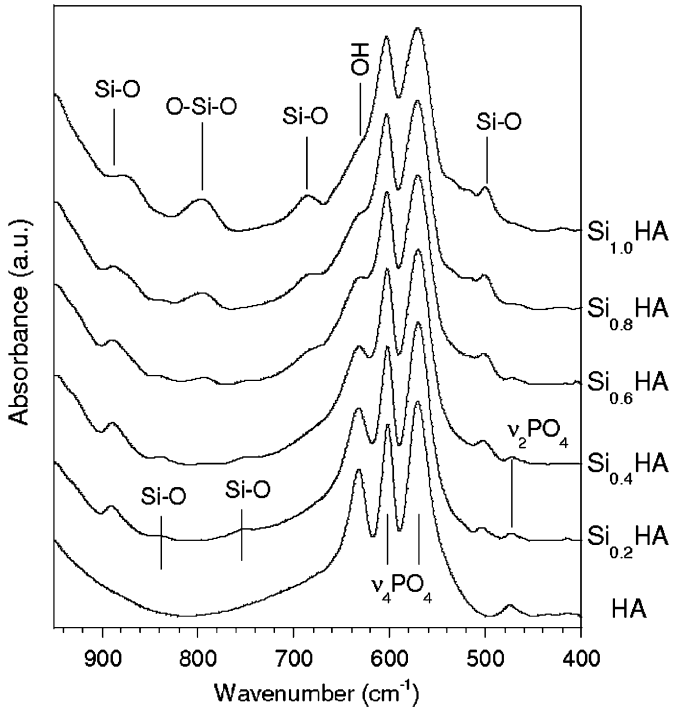

Fig. 9. FTIR spectra of Si_xHA ($x \leqslant 1$) powders heated at 1000 °C for 15 h.

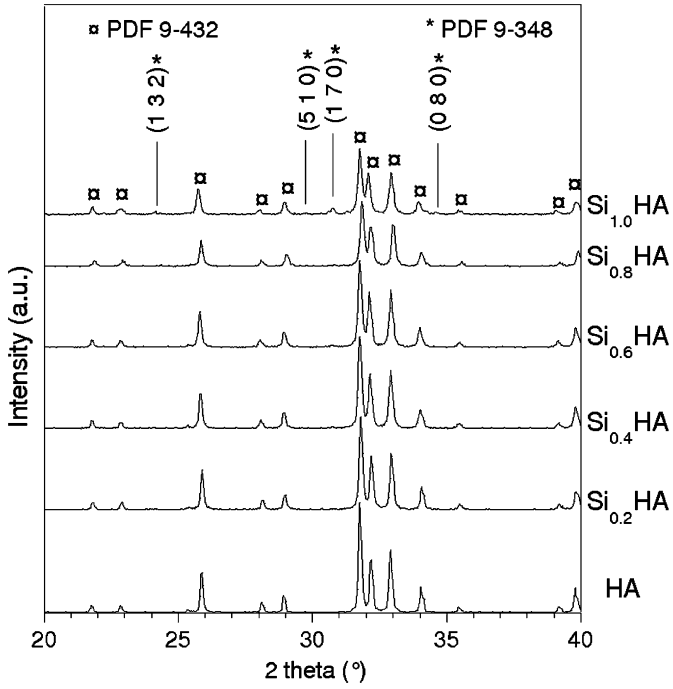

Fig. 10. XRD patterns of Si_xHA ($x \leqslant 1$) powders heated at 1000 °C for 15 h.

5. Conclusion

The powders containing more than 1.0 mol of silicon were always composed of two phases even after calcination. Only pure silicated hydroxyapatites $Ca_{10}(PO_4)_{6-x}(SiO_4)_x(OH)_{2-x}$ with

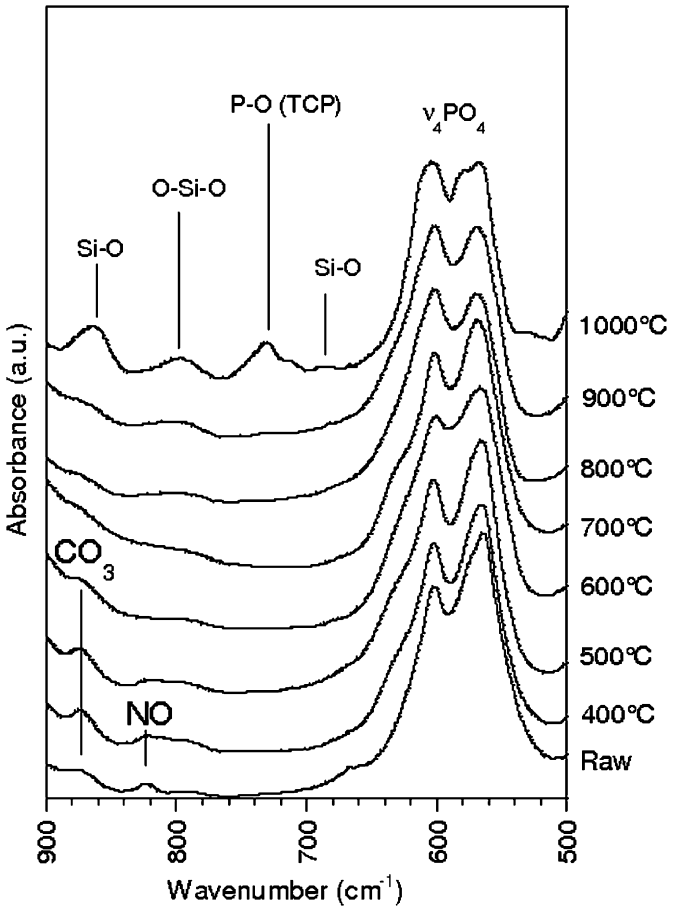

Fig. 11. FTIR spectra of $Si_{2.0}HA$ powder versus the temperature.

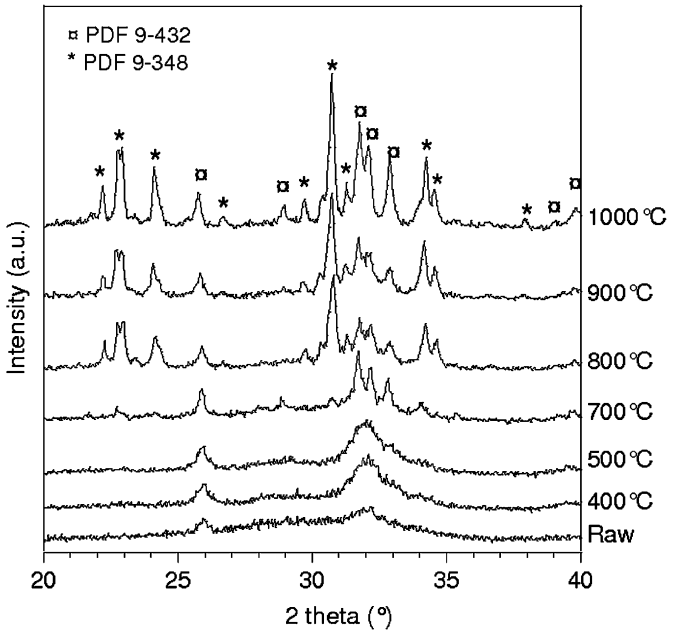

Fig. 12. XRD patterns of $Si_{2.0}HA$ powder versus the temperature.

$x \leqslant 1.0$ could be prepared successfully by this aqueous precipitation method followed by a heat treatment. The precipitated powders were composed of a partially carbonated and silicated

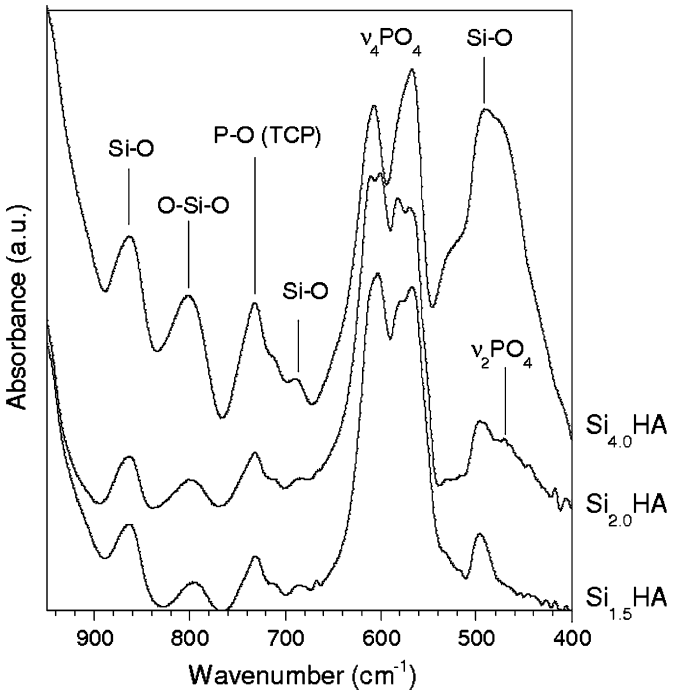

Fig. 13. FTIR spectra of Si_xHA powders ($x > 1$) heated at 1000 °C for 15 h.

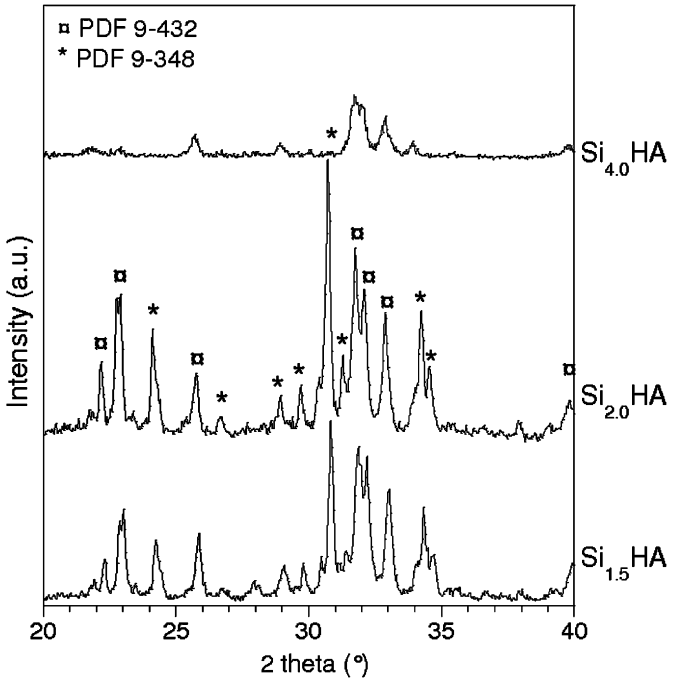

Fig. 14. XRD patterns of Si_xHA powders ($x > 1$) heated at 1000 °C for 15 h.

hydroxyapatites and a secondary phase containing silicon. The silicon was fully incorporated in the apatite during the calcination from 700 °C, silicate substituting for carbonate. Above 900 °C, pure silicated hydroxyapatites were produced. The mechanism of formation of these apatites was identified. The unit cell parameters of pure powders crystallized at 1000 °C were refined. This made it possible to calculate the bulk density, which was in agreement with the measured values. These powders were used to produce dense bioceramics and evaluate

Table 4
Silicon content, chemical formula, calculated density (D_x) and measured bulk density (ρ_c) of powders heat treated at 1000 °C for 15 h

Sample	Silicon content (mol)	Chemical composition	D_x (g cm^{-3})	ρ_c (g cm^{-3})
HA	0	$Ca_{10}(PO_4)_6(OH)_2$	3.154	3.14
$Si_{0.2}$HA	0.18	$Ca_{10}(PO_4)_{5.82}(SiO_4)_{0.18}(OH)_{1.82}$	3.133	3.11
$Si_{0.4}$HA	0.39	$Ca_{10}(PO_4)_{5.61}(SiO_4)_{0.39}(OH)_{1.61}$	3.119	3.11
$Si_{0.6}$HA	0.59	$Ca_{10}(PO_4)_{5.41}(SiO_4)_{0.59}(OH)_{1.41}$	3.102	3.11
$Si_{0.8}$HA	0.76	$Ca_{10}(PO_4)_{5.24}(SiO_4)_{0.76}(OH)_{1.24}$	3.083	3.09
$Si_{1.0}$HA	0.96	$Ca_{10}(PO_4)_{5.04}(SiO_4)_{0.96}(OH)_{1.04}$	3.071	3.06
$Si_{1.5}$HA		Apatite+α-TCP		
$Si_{2.0}$HA		Apatite+α-TCP		
$Si_{4.0}$HA		Crystallized+amorphous		

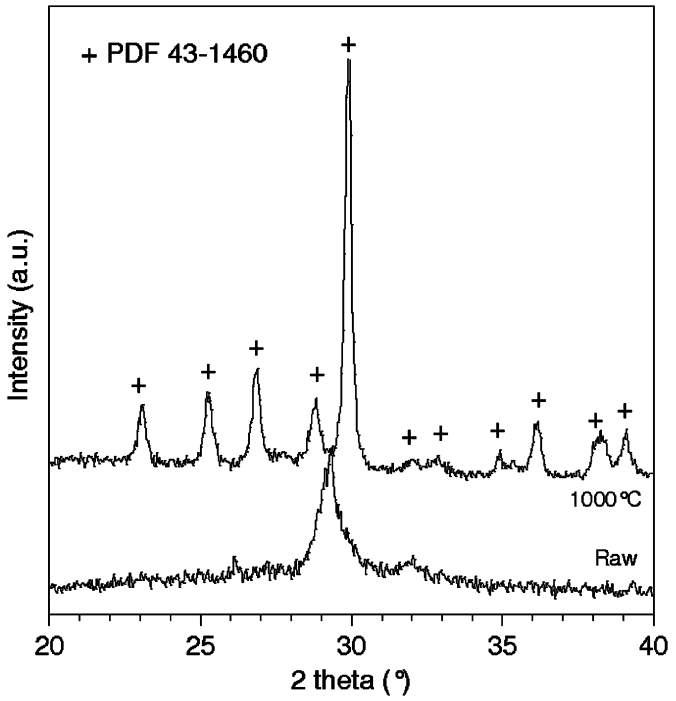

Fig. 15. XRD patterns of calcium silicate before and after heating at 1000 °C for 15 h.

the effect of silicate amount in the hydoxyapatite on its biological behaviour. This part of the study should be published in a forthcoming paper.

References

[1] L.L. Hench, J. Am. Ceram. Soc. 74 (1991) 1487–1510.
[2] M. Vallet-Regi, J.M. Gonzalez-Calbet, Prog. Solid State Chem. 32 (2004) 1–31.
[3] Y. Doi, T. Shibutani, Y. Moriwaki, T. Kajimoto, Y. Iwayama, J. Biomed. Mater. Res. 39 (1998) 603–610.
[4] J.E. Barralet, S.M. Best, W. Bonfield, J. Mat. Sci.: Mater. Med. 11 (2000) 719–724.
[5] J.P. Lafon, E. Champion, D. Bernache-Assollant, J. Eur. Ceram. Soc. 28 (2008) 139–147.
[6] M. Vallet-Regi, D. Arcos, J. Mater. Chem. 15 (2005) 1509–1516.
[7] I.R. Gibson, S.M. Best, W. Bonfield, J. Am. Ceram. Soc. 85 (2002) 2771–2777.
[8] F. Balas, J. Perez-Pariente, M. Vallet-Regi, J. Biomed. Mater. Res. 66A (2003) 364–375.
[9] N. Patel, S.M. Best, W. Bonfield, I.R. Gibson, K.A. Hing, E. Damien, P.A. Revell, J. Mat. Sci.: Mater. Med. 13 (2002) 1199–1206.
[10] J.L. Xu, K.A. Khor, J. Inorg. Biochem. 101 (2007) 187–195.
[11] A.E. Porter, N. Patel, J.N. Skepper, S.M. Best, W. Bonfield, Biomaterials 24 (2003) 4609–4620.
[12] E.S. Thian, J. Huang, S.M. Best, Z.H. Barber, W. Bonfield, Biomaterials 26 (2005) 2947–2956.
[13] E.S. Thian, J. Huang, S.M. Best, Z.H. Barber, R.A. Brooks, N. Rushton, W. Bonfield, Biomaterials 27 (2006) 2692–2698.
[14] A.E. Porter, T. Buckland, K. Hing, S.M. Best, W. Bonfield, J. Biomed. Mater. Res. B: Appl. Biomater. 76B (2006) 25–33.
[15] A.E. Porter, Micron 37 (2006) 681–688.
[16] A.J. Ruys, J. Austr. Ceram. Soc. 29 (1993) 71–80.
[17] D. Arcos, J. Rodriguez-Carvajal, M. Vallet-Regi, Solid State Sci. 6 (2004) 987–994.
[18] Y. Tanizawa, T. Suzuki, Phosphorus Res. Bull. 4 (1994) 83–88.
[19] X.L. Tang, X.F. Xiao, R.F. Liu, Mater. Lett. 59 (2005) 3841–3846.
[20] I.R. Gibson, S.M. Best, W. Bonfield, J. Biomed. Mater. Res. 44 (1999) 422–428.
[21] D. Arcos, J. Rodriguez-Carvajal, M. Vallet-Regi, Chem. Mater. 16 (2004) 2300–2308.
[22] S.R. Kim, J.H. Lee, Y.T. Kim, D.H. Riu, S.J. Jung, Y.J. Lee, S.C. Chung, Y.H. Kim, Biomaterials 24 (2003) 1389–1398.
[23] T. Leventouri, C.E. Bunaciu, V. Perdikatsis, Biomaterials 24 (2003) 4205–4211.
[24] C. Rey, B. Collins, T. Goehl, I.R. Dickson, M.J. Glimcher, Calcif. Tissue Int. 45 (1989) 157–164.
[25] R.A. Young, The Rietveld method, Oxford Science Publications, Oxford, 1995.
[26] J. Rodriguez-Carvajal, FULLPROF98, Version 0.2, Laboratoire L. Brillouin, Grenoble, 1998.
[27] D. Dunfield, M. Sayer, H.F. Shurvell, J. Phys. Chem. B 109 (2005) 19579–19583.
[28] M.Y. Koh, G. Kawachi, K. Kikuta, M. Kamitakahara, C. Ohtsuki, J. Ceram. Soc. Japan 115 (2007) 732–737.
[29] A. Jillavenkatesa, R.A. Condrate, Spectros. Lett. 31 (1998) 1619–1634.
[30] J.E. Barralet, S.M. Best, W. Bonfield, J. Biomed. Mater. Res. 41 (1998) 79–86.
[31] S. Raynaud, E. Champion, D. Bernache-Assollant, P. Thomas, Biomaterials 23 (2002) 1065–1072.